JOURNAL OF CHEMICAL & ENGINEERING DATA

ARTICLE

pubs.acs.org/jced

Removal of Mercury Ions from Ethanol Solution Using Silica Gel Functionalized with Amino-Terminated Dendrimer-Like Polyamidoamine Polymers: Kinetics and Equilibrium Studies

Changmei Sun, Fang Ma, Guanghua Zhang, Rongjun Qu,* and Ying Zhang

School of Chemistry and Materials Science, Ludong University, Yantai 264025, China

ABSTRACT: The potential use of silica gel functionalized with dendrimer-like, amino-terminated polyamidoamine polymers (PAMAM) as adsorbents for the removal of mercury ions from ethanol solution was evaluated. The adsorption isotherm and adsorption kinetics were investigated by using the batch method. The adsorption capacity was found to depend on the generation number of PAMAM loaded, contact time, initial concentration, and temperature. The experimental data were fitted to pseudofirst-order and pseudosecond-order kinetic models. The results indicated that all of the adsorption data fitted well with the second-order kinetic model. A stepped fitting method was adopted to determine whether intraparticle diffusion or external diffusion was the rate-limiting step. The adsorption isotherms were fitted by the Langmuir model, Freundlich model, and Dubinin−Radushkevich (D-R) model. The results showed that the Langmuir model defined the equilibrium data better than the Freundlich model. From the D-R isotherm model, the calculated mean free energy E showed that the adsorptions occurred via chemical processes. The thermodynamic parameters of ΔG^0, ΔH^0, and ΔS^0 indicated that the Hg^{2+} adsorption was endothermic and spontaneous with decreased randomness at the solid−solution interface.

1. INTRODUCTION

It has been well-documented that mercury is a pervasive contaminant that is highly toxic and is readily accumulated by organisms.[1] Generally, mercury is released to the environment from both natural activities including weathering of mercury-containing areas, the degassing from surface water and from the Earth's crust through volcanic eruptions, naturally caused forest fires, and biogenic emissions,[2] and anthropogenic activities including agriculture, battery production, fossil fuel burning, mining and metallurgical processes, paint and chloralkali industries, and wood pulping.[3] The World Health Organization (WHO) recommends a maximum uptake of 0.3 mg per week and 1 $\mu g \cdot L^{-1}$ as the maximum acceptable concentration in drinking water.[4] To remove mercury ions from wastewater before it is released into the environment, a number of technologies have been developed including chemical precipitation, reverse osmosis, evaporation, membrane filtration, adsorption biological treatment, ion exchange, and adsorption.[5] Among these, selective adsorption utilizing biological materials, mineral oxides, carbon, or polymer resins has generated much interest among researchers and environmental engineers and scientists.[6−10]

However, most of the research focused mainly on the removal of mercury in aqueous solution (industrial wastewater) rather than nonaqueous solution such as gasoline or ethanol fuel solution. In fact, the combustion of fuels to produce electricity and heat is the major source of atmospheric emissions of Hg on a global scale.[11] Since the majority of Hg emissions from fuel combustion is in the gaseous phase, it is difficult to remove once it diffuses into the atmosphere.[12] Moreover, the presence of Hg in ethanol fuel might affect processing, where mercury can react with metallic surfaces, form amalgams, and impair the proper operation of the equipment.[13] Catalyst poisoning was also reported.[14] Therefore, the removal of metal ions, especially Hg in ethanol fuel, has become a key driving force for the development of novel adsorbents with low cost and high adsorption capabilities for metal ions in ethanol. Gushikem and co-workers were the first to report the adsorption and preconcentration capabilities of silica gel modified by imidazole for Cu, Ni, Fe, Zn, Cd, and Mn in ethanol.[15,16] Afterward, Filho et al. synthesized a series of modified silica with heterocyclic functional groups to adsorb metal ions such as Mn and Ni in ethanol solution.[17−19] We noticed that most of the adsorbents reported involved heterocyclic functional groups, while those with other types of functional groups were rare. In addition, the adsorption mechanism and kinetics as well as the removal of Hg from ethanol solution were seldom reported.

Our goal was to develop novel adsorbents for the removal of Hg from ethanol fuel solution. We chose to immobilize polyamidoamine (PAMAM) dendrimers, which are highly branched and well-defined polymers with unique topology structure versatile physicochemical properties, as functional groups.[20−22] The PAMAM polymers were loaded onto silica gel, and the adsorbents obtained were evaluated for their capability to remove mercury ions from ethanol solution. Furthermore, equilibrium and kinetic studies were also conducted.

2. EXPERIMENTAL SECTION

2.1. Materials and Methods. Silica gel functionalized with amino-terminated dendrimer-like PAMAM polymers (SiO_2-G1.0, SiO_2-G2.0, SiO_2-G3.0, and SiO_2-G4.0) was prepared according to our previous work[23] as shown in Figure 1. The parameters

Special Issue: Kenneth N. Marsh Festschrift

Received: March 16, 2011
Accepted: June 13, 2011
Published: June 29, 2011

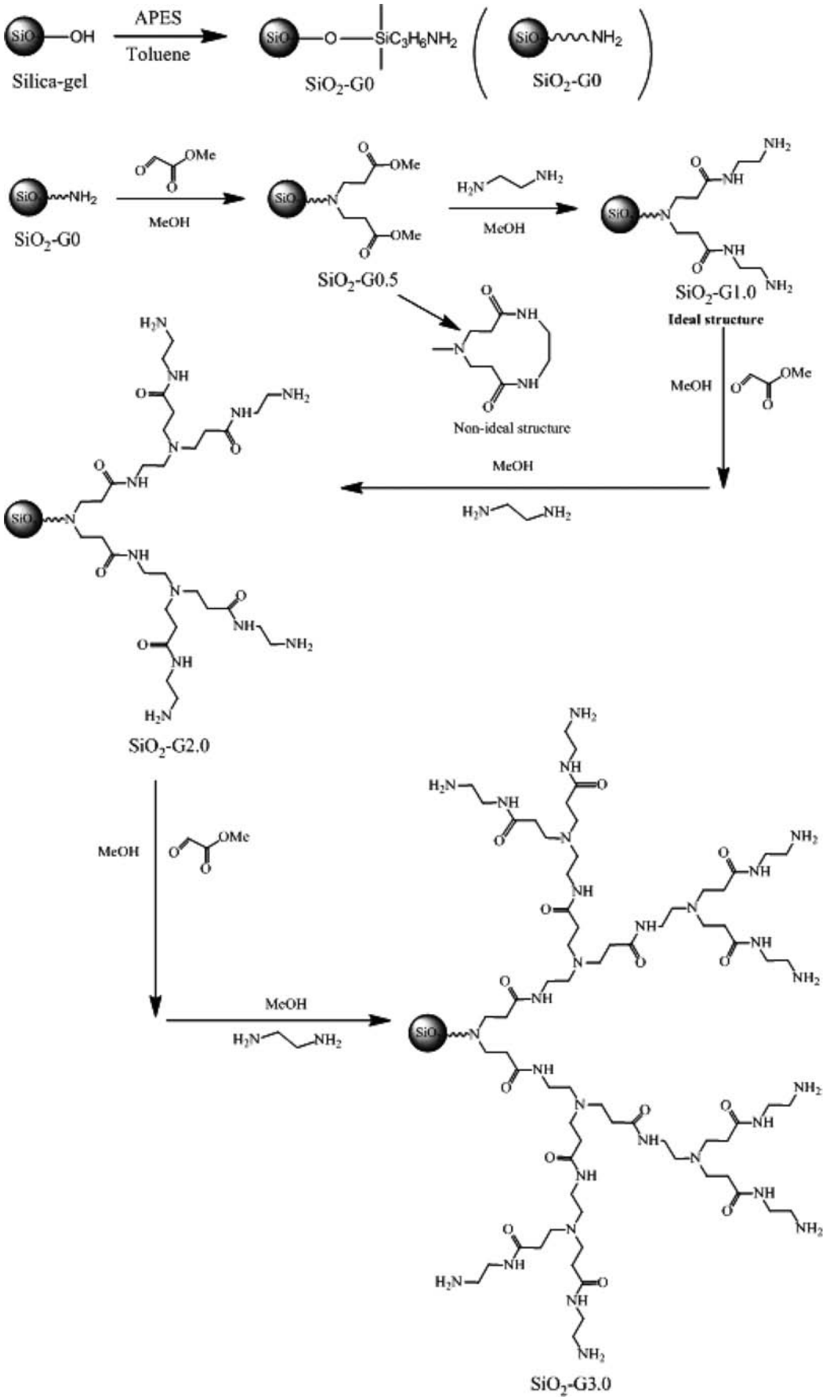

Figure 1. Synthesis of SiO_2-G1.0, SiO_2-G2.0, and SiO_2-G3.0.

dx.doi.org/10.1021/je200235j |*J. Chem. Eng. Data* 2011, 56, 4407–4415

Table 1. Brunauer–Emmett–Teller (BET) Surface Area (s_{BET}), Barrett–Joyner–Halenda (BJH) Desorption Average Pore Diameter (d), and Grafting Percentage (GP) of the Four Resins SiO_2-G1.0, SiO_2-G2.0, SiO_2-G3.0, and SiO_2-G4.0

resin	s_{BET}	d	GP
	$m^2 \cdot g^{-1}$	nm	%
SiO_2-G1.0	266.55	7.35	10.49
SiO_2-G2.0	157.16	5.86	19.83
SiO_2-G3.0	121.16	5.76	27.65
SiO_2-G4.0	42.73	5.02	42.94

of the four resins are listed in Table 1. Stock solutions of Hg^{2+}, Cu^{2+}, Fe^{3+}, Co^{2+}, and Ni^{2+} were prepared by dissolving the corresponding $HgCl_2 \cdot 2H_2O$, $CuCl_2 \cdot 2H_2O$, $FeCl_3 \cdot 2H_2O$, $CoCl_2 \cdot 6H_2O$, and $NiCl_2 \cdot 6H_2O$ in dry ethanol. All reagents were analytical grade and used without further purification.

The concentrations of metal ions were determined using a 932B-model atomic absorption spectrometer (AAS, GBC, Australia) equipped with an air–acetylene flame. The operating parameters were as follows: lamp current, 3.0 mA; slit width, 0.5 nm; wavelength, 253.7 nm; sensitivity, 1.60 $\mu g \cdot g^{-1}$.

2.2. Static Adsorption Experiments. Static adsorption experiments were carried out by shaking the adsorbent (0.05 g) in 0.001 $mol \cdot kg^{-1}$ ethanolic metal solution (20 mL) at 100 rpm for 24 h at room temperature. After adsorption, an aliquot (10 mL) was removed and analyzed by AAS to determine the metal ion concentration. The amount of metal adsorbed was calculated according to eq 1:

$$Q = \frac{(C_0 - C)V}{W} \quad (1)$$

where Q is the adsorption amount, $mmol \cdot g^{-1}$; C_0 is the initial metal ion concentration, $mol \cdot kg^{-1}$; C is the final metal ion concentration, $mol \cdot kg^{-1}$; V is the volume, L; and W is the weight of adsorbents, g.

2.3. Effect of Adsorbent Loading on Adsorption. To study the effect of adsorbent loading, a series of 0.001 $mol \cdot kg^{-1}$ ethanolic metal solutions (20 mL) was treated with various amounts of adsorbent (ranging from 10 mg to 60 mg) and equilibrated for 24 h at room temperature. The percent removal of metal ions was calculated according to eq 2

$$PR(\%) = (C_0 - C)/C_0 \cdot 100 \quad (2)$$

2.4. Adsorption Kinetics. The adsorption kinetics was studied using a batch method by treating the adsorbents (0.03 g) in 1.0 mM ethanolic metal solution (20 mL) at (278 to 298) K. At various time intervals, an aliquot (10 mL) of the solution was removed, and the metal ion concentration was determined by AAS.

2.5. Adsorption Isotherms. The adsorption isotherms were investigated by treating the adsorbents (0.03 g) with various concentrations of different metal ion solutions for 24 h at (278 to 298) K.

2.6. Effect of Metal Ion Concentration on Adsorption. The effect of metal ion concentration was studied by treating the adsorbent (0.030 g) with 20 mL ethanolic solutions containing various initial metal ion concentrations (0.1 to 1.0) $mmol \cdot kg^{-1}$ and equilibrated for 24 h at room temperature.

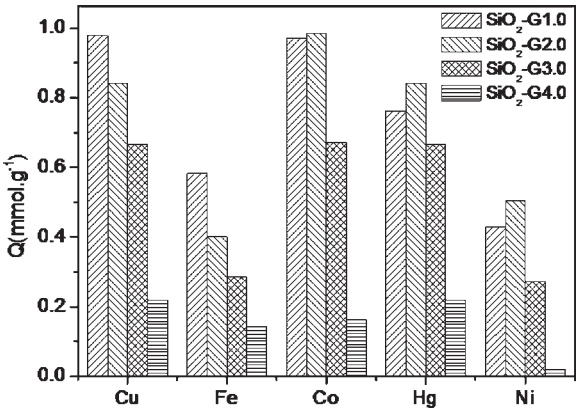

Figure 2. Saturated adsorption amounts of SiO_2-G1.0 to SiO_2-G4.0 for metal ions in ethanol solution (initial metal ion concentration: 0.001 $mol \cdot kg^{-1}$; volume of solution: 20 mL; equilibration time: 24 h).

3. RESULTS AND DISCUSSION

3.1. Static Saturated Adsorption Amounts. The saturated adsorption amount of metal ions is generally considered as one of the most critical parameters for evaluating adsorbent capability. Base metal ions such as Cu^{2+}, Hg^{2+}, Co^{2+}, Fe^{3+}, and Ni^{2+} that are often found in ethanol fuel were selected to investigate the adsorption properties of SiO_2-G1.0 to SiO_2-G4.0 by using a static method. The results are shown in Figure 2.

Theoretically, the adsorption capacity of the adsorbent for metal ions should increase with increasing generation number of dendrimer-like PAMAM due to the increase in N atom number and functional groups. However, the adsorption capability of the PAMAM modified adsorbent was found to decrease with increasing generation number. This may be attributed to the higher steric hindrance and cross-linking degree inherent in PAMAM with higher generation number, which obstructs metal ions from diffusing into the interior of PAMAM to contact with interior functional groups.

Owing to its toxicity and harmful environmental effects and the lack of studies on its removal from ethanol solution, Hg^{2+} was chosen for the adsorption kinetics and isotherm studies of SiO_2-G1.0, SiO_2-G2.0, and SiO_2-G3.0 in ethanol solution. Since the adsorption of metal ions was very low for SiO_2-G4.0, the adsorption performance of SiO_2-G4.0 was not studied further.

3.2. Effect of Resin Loading on Adsorption. The effect of resin loading on the removal of Hg^{2+} by SiO_2-G1.0, SiO_2-G2.0, and SiO_2-G3.0 in ethanol solution is shown in Figure 3. Resin loading was varied from 10 mg to 60 mg, and the mixture containing an initial mercury concentration of 0.001 $mol \cdot kg^{-1}$ was equilibrated for 24 h. It was apparent that the equilibrium adsorption amount decreased and the removal percent increased with increasing resin loading. This was anticipated because, for a fixed initial solute concentration, increasing the adsorbent loading would provide greater surface area (or adsorption sites).[24,25] Moreover, it can be seen that SiO_2-G1.0 could remove mercury ions more effectively than SiO_2-G2.0 and SiO_2-G3.0. When the resin loading was 30 mg, the removal percent of SiO_2-G1.0 almost reached 100%, while those of SiO_2-G2.0 and SiO_2-G3.0 were only about 70% and 60%, respectively. When the loading of SiO_2-G2.0 and SiO_2-G3.0 was increased to 60 mg, the removal of Hg^{2+} reached ~90%.

3.3. Adsorption Kinetics and Mechanism. The adsorption kinetics study could provide information about the adsorption

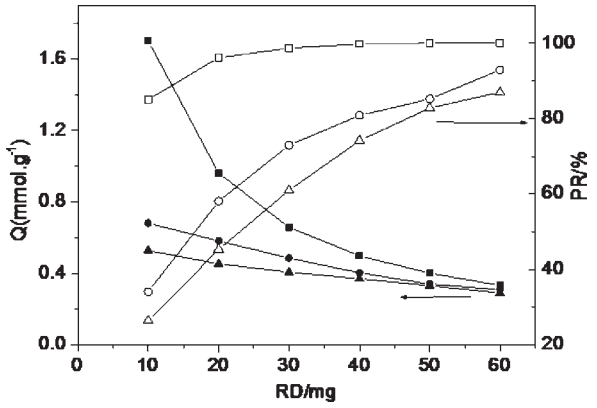

Figure 3. Effect of resin dosage (RD) on the adsorption amount of Hg^{2+} onto ■, SiO_2-G1.0; ●, SiO_2-G2.0; and ▲, SiO_2-G3.0 and the percent removal (PR) for Hg^{2+} of □, SiO_2-G1.0; ○, SiO_2-G2.0, and △, SiO_2-G3.0 (initial metal ion concentration: 0.001 mol·kg^{-1}; volume of solution: 20 mL; equilibration time: 24 h).

mechanism, which is important for optimizing the efficiency of the process. Successful application of the adsorption demands innovation of cheap, easily available, and abundant adsorbents of known kinetic parameters and adsorption characteristics. Figure 4 shows the kinetic curves of SiO_2-G1.0, SiO_2-G2.0, and SiO_2-G3.0 for the adsorption of Hg^{2+}. The results show that the adsorption was fast before 100 min and then approaching equilibrium. The time profiles of the adsorptions were single, smooth, and continuous curves leading to saturation, suggesting the possible monolayer coverage of Hg^{2+} on the surface of the three resins.[26]

The adsorption was significantly affected by the temperature of the mixtures. As could be seen from Figure 4, the adsorption capacities increased with increasing temperature. Possible explanations for this are: (1) the resins could be swollen more completely at higher temperatures, which facilitated the diffusion of Hg^{2+} into the resins; (2) the adsorption was an endothermic process and thus favors high temperature conditions. In addition, it was noticed that the adsorptions of the resins at 298 K was accelerated after ~200 min, which might be due to the sufficient swelling of the resins with prolonged time and high temperature.

Adsorption kinetics can be modeled by several models, including the pseudofirst-order Lagergren equation[27]and pseudosecond-order rate equation[28] given below as eqs 3 and 4, respectively.

$$\log(q_e - q_t) = \log q_e - \frac{k_1}{2.303} t \quad (3)$$

$$\frac{t}{q_t} = \frac{1}{k_2 q_e^2} + \frac{1}{q_e} t \quad (4)$$

where k_1 is the rate constant of pseudofirst-order adsorption, k_2 is the rate constant of pseudosecond-order adsorption, and q_e and q_t are the adsorption amount at equilibrium and at time t, respectively.

For the pseudofirst-order kinetic model, eq 3 can be transformed to eq 5, which can be used to predict the adsorption equilibrium. The constants (k_1 and q_e) obtained from nonlinear fitting results are given in Table 2.

$$q_t = q_e(1 - e^{-k_1 t}) \quad (5)$$

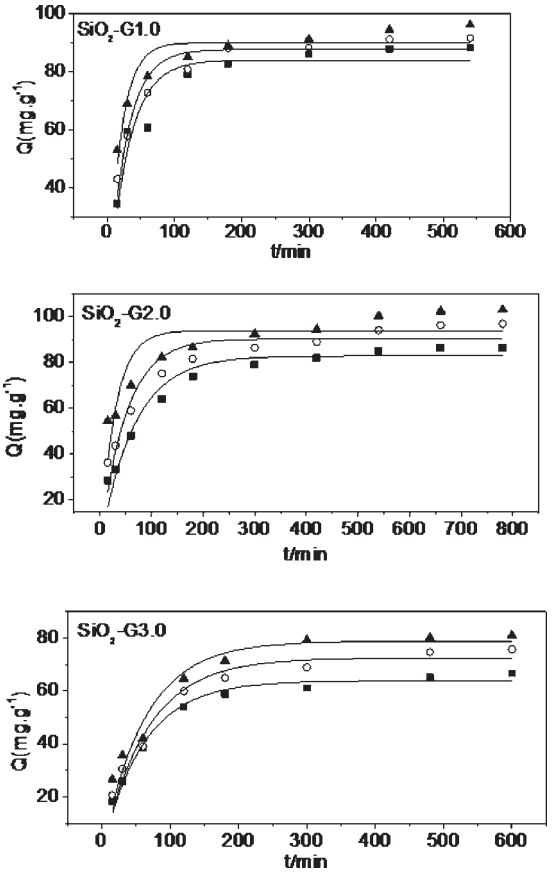

Figure 4. Adsorption kinetics of Hg^{2+} onto SiO_2-G1.0, SiO_2-G2.0, and SiO_2-G3.0 resins and pseudofirst-order kinetic model (solid line; initial metal ion concentration: 0.001 mol·kg^{-1}; volume of solution: 20 mL; equilibration time: 24 h; temperature: ■, 278 K; ○, 288 K; and ▲, 298 K).

For pseudosecond-order kinetic model, the constants can be obtained from plotting (t/q_t) versus t. The values k^2 and q_e are also given in Table 2. Figures 4 and 5 present the curves for fitting experimental data at different temperatures using pseudofirst-order and pseudosecond-order kinetic models. The results show that the first-order kinetic model was not as good as the second-order kinetics in modeling the kinetics and the regression coefficients were also lower in comparison (Table 2). Furthermore, the equilibrium adsorption from the pseudosecond-order model was much closer to the experimental data, suggesting that the second-order kinetics model is better.

On the basis of the pseudosecond-order kinetic model, the initial adsorption rate (h) and half adsorption time ($t_{1/2}$) were estimated (Table 2) according to the following eqs 6 and 7.[29] Half adsorption time, the time required for the resins to uptake half of the amount adsorbed at equilibrium, is often considered as a measure of the rate of adsorption.[30]

$$h = k q_e^2 \quad (6)$$

$$t_{1/2} = \frac{1}{k q_e} \quad (7)$$

The data in Table 2 show that the initial adsorption rate h increased with temperature, probably because of the faster diffusion rate of Hg^{2+} under higher temperatures. Among the

Table 2. Kinetic Parameters Obtained from Pseudofirst-Order and Pseudodecond-Order Models for Hg^{2+} onto SiO_2-G1.0, SiO_2-G2.0, and SiO_2-G3.0 Resins at Different Temperatures

		pseudofirst-order model				pseudosecond-order model				
		$q_{e,exp}$	$q_{e,cal}$	k_1		$q_{e,cal}$	k_2	h	$t_{1/2}$	
resin	T/K	mg·g^{-1}	mg·g^{-1}	min^{-1}	R^2	mg g^{-1}	10^4 g·mg^{-1}·min^{-1}	mg·g^{-1}·min^{-1}	min	R^2
SiO_2-G1.0	278	88.34	84.05	0.03307	0.9104	92.59	4.73	4.05	22.83	0.9995
	288	91.72	87.76	0.03680	0.9433	95.24	5.66	5.13	18.55	0.9998
	298	96.22	90.13	0.05126	0.8935	98.04	6.47	6.22	15.76	0.9996
SiO_2-G2.0	278	86.48	82.87	0.01517	0.9485	91.74	2.29	1.93	47.60	0.9987
	288	96.86	90.32	0.02011	0.9119	101.01	2.40	2.45	41.25	0.9986
	298	103.58	93.92	0.03411	0.7345	106.38	2.93	3.32	32.08	0.9978
SiO_2-G3.0	278	66.67	63.81	0.01625	0.9832	71.90	2.95	1.53	47.15	0.9993
	288	75.65	72.43	0.01508	0.9680	81.97	2.37	1.59	51.48	0.9989
	298	80.98	78.75	0.01596	0.9431	87.72	2.59	1.99	44.02	0.9979

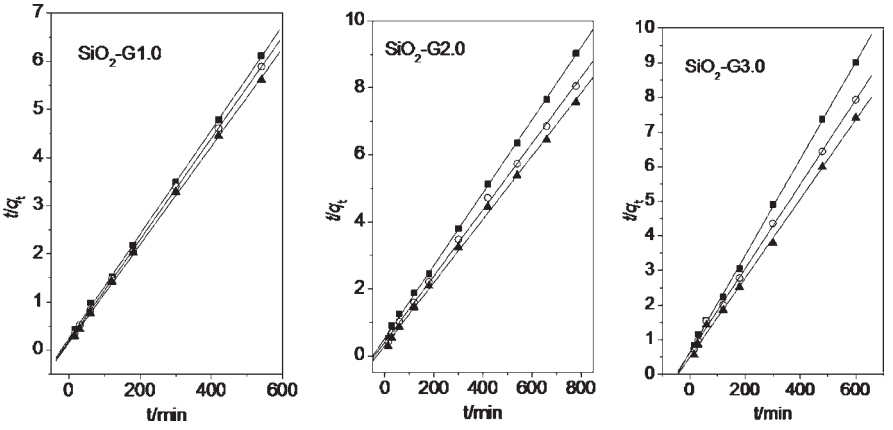

Figure 5. Pseudosecond-order kinetic plots of Hg^{2+} onto SiO_2-G1.0, SiO_2-G2.0, and SiO_2-G3.0 resins at ■, 278 K; ○, 288 K; and ▲, 298 K.

resins, the h values decreased in the following order: SiO_2-G1.0 > SiO_2-G2.0 > SiO_2-G3.0. This could be attributed to the increase in generation number of PAMAM, where cross-linking of the functional groups increases with each generation and resulted in greater steric hindrance. Thus, the diffusion of Hg^{2+} became slower, and the corresponding h values were decreased.

The values of k_2 and $t_{1/2}$ reflect the speed of adsorption equilibrium. For SiO_2-G1.0 and SiO_2-G2.0, the k_2 values increased, and $t_{1/2}$ decreased with temperature, indicating that the higher temperature favors adsorption. Hence, the time required for the resins to reach adsorption equilibrium became shorter at higher temperatures. However, the adsorption behavior of SiO_2-G3.0 was different, in which the order of k_2 values was 278 K > 298 K > 288 K. This phenomenon may be due to the structure of PAMAM loaded on the SiO_2-G3.0 resin. Since the molecular volume of G3.0 PAMAM and the cross-linking degree was much higher than SiO_2-G1.0 and SiO_2-G2.0, the PAMAM groups on SiO_2-G3.0 tend to intertwine together and become compact. At low temperatures (278 K), the mobility of PAMAM groups was weak, and the chains were intertwined, which prevented the diffusion of solvent molecules, and the resin did not swell enough. As a result, only the surface functional groups were able to interact with Hg^{2+}, but not inside the resin. Therefore, adsorption equilibrium could be attained in a relative short period of time. When the temperature was increased to 288 K, the mobility of PAMAM groups became greater, and solvent molecules could pass through the flexible functional groups and diffuse into the resin to make it swell. Accordingly, Hg^{2+} was able to diffuse into the resin and contact with the inner functional groups. Because of the additional internal adsorption, the time required for the resin to reach adsorption equilibrium became longer than that at 278 K. When the temperature was further increased to 298 K, the resin could be swollen more sufficiently and promote the diffusion of Hg^{2+}. Moreover, the diffusion rate of Hg^{2+} is also faster at a higher temperature. Thus, the adsorption equilibrium time at 298 K was the shortest. We also observed similar behavior during the adsorption of other metal ions such as Cu^{2+} and Fe^{3+} with the same resin in ethanol solution, which will be discussed in another paper.

In aqueous solution, the order of the adsorption capacity for Hg^{2+} was: SiO_2-G1.0 < SiO_2-G2.0 < SiO_2-G3.0,[23] which was quite different than the adsorption in ethanol solution. The adsorption mechanism in ethanol solution might be different to that in water solution. In ethanol solution, Hg^{2+} ions may be solvated by ethanol as shown in Figure 6. The volume of a solvated Hg^{2+} ion is very large, and the diffusion rate of such big molecule may be significantly affected by external factors, such as temperature and cross-linking degree of functional groups. As

dx.doi.org/10.1021/je200235j |J. Chem. Eng. Data 2011, 56, 4407–4415

shown in Figure 6, a solvated Hg^{2+} ion may consist of two parts, an organic layer formed by $-CH_2CH_3$ groups and an inorganic layer formed by $-OH$ group and Hg^{2+} ion. Consequently, two kinds of interactions probably occurred during the adsorption process. A chemical interaction (complexation) may exist between the Hg^{2+} inorganic layer and N atoms in PAMAM group; a physical adsorption may exist between the Hg^{2+} organic layer and the organic chain in PAMAM group according to the theory of "similarity and intermiscibility", which suggests that similar substances are more likely to be dissolved by each other.

Our data (Table 2) indicate that SiO_2-G2.0 possessed the highest adsorption capacities among the resins at higher temperatures (298 K or 288 K). This could be explained by the fact that, at higher temperatures, the salvation degree of Hg^{2+} became weaker, where some ethanol molecules might be desorbed from Hg^{2+}. As a result, the volume of a solvated Hg^{2+} ion became smaller, making it easier to diffuse into the resin and react with the inner functional groups. For SiO_2-G3.0, the cross-linking degree of PAMAM was much higher than that of SiO_2-G2.0, and the pore size in SiO_2-G3.0 was smaller for Hg^{2+} ions to diffuse into the resin. Therefore, the adsorption capacity of SiO_2-G3.0 was lower than SiO_2-G2.0. For SiO_2-G1.0, the grafting of PAMAM was lower and resulted in a lower adsorption capacity as compared to SiO_2-G2.0.

The adsorption process on a porous adsorbent typically involves three stages: (i) external diffusion, (ii) internal diffusion (also called intraparticle diffusion), and (iii) actual adsorption.[31] It is generally accepted that stage (iii) is very rapid and dose not represent the rate-determining step in the uptake of organic/inorganic compounds.[32] For the other two steps in the overall adsorption process, their rates can vary as follows:

case I: external diffusion > internal diffusion;
case II: external diffusion < internal diffusion; and
case III: external diffusion ≈ internal diffusion.

In cases I and II, the rate is governed by film and particle diffusion, respectively. In case III, the diffusion of ions to the boundary may not be possible at a significant rate, leading to the formation of a liquid film with a concentration gradient surrounding the adsorbent particles.[33] An internal diffusion model based on Flick's second law is often used to test whether the internal diffusion step is the rate-limiting step.[34] The intraparticle diffusion model is represented as:

$$q_t = k_{int} t^{0.5} \quad (8)$$

where k_{int} is the intraparticle diffusion rate constant. If intraparticle diffusion is involved in the adsorption process, then the plot of the square root of time against uptake (q_t) would result in a linear relationship and the intraparticle diffusion would be the rate-limiting step if this line passes through the origin.

The data were analyzed by stepped fitting method, where the q_t values before and after 120 min were fitted by the intraparticle diffusion model (eq 8). The results are summarized in Table 3, and the fitting curves for the adsorption of Hg^{2+} by SiO_2-G3.0 at 278 K are shown in Figure 7. The data show that the fitted lines passed through the origin in step I, indicating that intraparticle diffusion may be the rate-limiting step in this process. Moreover, it can be seen that the k_{int} values of the three resins increased with increasing temperature. This could be that the functional groups became more flexible at higher temperature and allowed Hg^{2+} to diffuse into the interior of the resin more easily, because of the weaker diffusion resistance caused by the functional groups. Furthermore, the R^2 values in step I at higher temperatures (298 K) for the three resins were much lower than those at lower temperatures (278 K and 288 K), which probably indicated that intraparticle diffusion was not the rate-limiting step at high temperature because of the same reason. We also found that in step I, the k_{int} values of the three resins decreased in the following order: SiO_2-G1.0 > SiO_2-G2.0 > SiO_2-G3.0. This is consistent

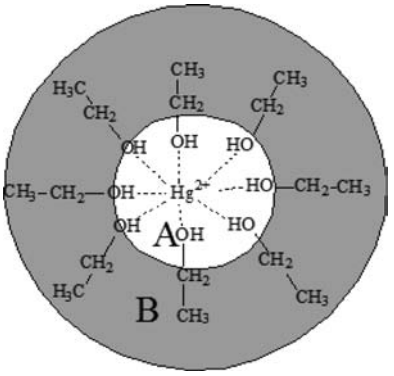

Figure 6. Schematic diagram of Hg^{2+} ions solvated by ethanol (A: inorganic layer; B: organic layer).

Table 3. Parameters of the Intraparticle Diffusion Model for Hg^{2+} onto SiO_2-G1.0, SiO_2-G2.0, and SiO_2-G3.0 Resins at Different Temperatures

		A			B		
			k_{int}			k_{int}	
resin	T/K	eq 1	mg·g^{-1}·min$^{-1/2}$	R^2	eq 2	mg·g^{-1}·min$^{-1/2}$	R^2
SiO_2-G1.0	278	$q_t = 8.8576t^{0.5}$	8.86	0.9869	$q_t = 0.5771t^{0.5} + 75.499$	0.58	0.9427
	288	$q_t = 9.9827t^{0.5}$	9.98	0.9831	$q_t = 0.4109t^{0.5} + 82.204$	0.41	0.9572
	298	$q_t = 11.35t^{0.5}$	11.35	0.9403	$q_t = 0.8633t^{0.5} + 76.516$	0.86	0.9771
SiO_2-G2.0	278	$q_t = 6.0681t^{0.5}$	6.07	0.9855	$q_t = 0.9009t^{0.5} + 62.845$	0.90	0.9473
	288	$q_t = 7.3775t^{0.5}$	7.38	0.9872	$q_t = 1.1182t^{0.5} + 66.788$	1.11	0.9775
	298	$q_t = 8.7323t^{0.5}$	8.73	0.8260	$q_t = 1.2608t^{0.5} + 69.408$	1.26	0.9779
SiO_2-G3.0	278	$q_t = 4.8853t^{0.5}$	4.89	0.9990	$q_t = 0.7217t^{0.5} + 49.042$	0.72	0.9920
	288	$q_t = 5.3605t^{0.5}$	5.36	0.9954	$q_t = 1.0154t^{0.5} + 51.451$	1.02	0.9825
	298	$q_t = 5.9163t^{0.5}$	5.92	0.9828	$q_t = 0.2429t^{0.5} + 74.929$	0.24	0.9760

with the order of the h values for the three resins (Table 2) and that the pseudosecond-order kinetic model was reasonable.

In step (II), most R^2 values were above 0.95, but the fitting straight lines did not pass through the origin, indicating that intraparticle diffusion was involved in this process, but it was no longer the rate-limiting step. In addition, the k_{int} values were much smaller than those in step I, which indicated that intraparticle diffusion was weaker in step II and the rate-limiting step was attributed to external diffusion. Moreover, the slower adsorption rate was inevitable in the final adsorption process since the number of adsorption sites was reduced.

3.4. Adsorption Isotherm. Adsorption isotherms are important for the description of how adsorbate will interact with an adsorbent and are critical in optimizing the use of an adsorbent. To investigate the adsorption isotherms, three equilibrium models, the Langmuir, Freundlich, and Dubinin−Radushkevich (D-R) isotherm models, were analyzed.

The well-known linear form of the Langmuir model is as follows:

$$\frac{C_e}{q_e} = \frac{1}{q_{max}b} + \frac{C_e}{q_{max}} \quad (9)$$

where q_e is the equilibrium metal ion concentration on the adsorbent, C_e is the equilibrium metal ion concentration in the solution, q_{max} is the monolayer adsorption capacity of the adsorbent, and K_L is the Langmuir adsorption constant, which relates to the adsorption energy. The Langmuir equation is applicable to homogeneous adsorption, where the adsorption of each adsorbate molecule onto the surface has equal adsorption activation energy.

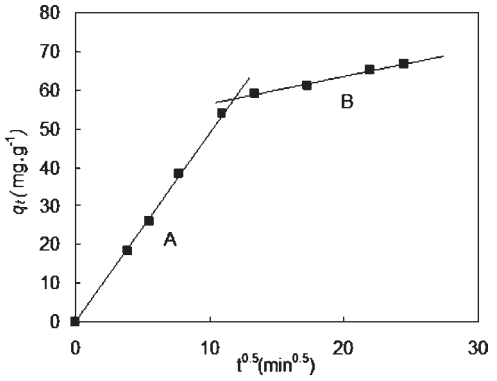

Figure 7. Intraparticle diffusion plots for adsorption of mercury on SiO_2-G3.0 at 278 K (A; step I, linear equation: $q_t = 4.8853t^{0.5}$; B: step II, linear equation: $q_t = 0.7217t^{0.5} + 49.042$).

The linear form of the Freundlich model is given as:

$$\log q_e = \log k_F + \frac{1}{n}\log C_e \quad (10)$$

where k_F is a constant indicative of the adsorption capacity of the adsorbent and $1/n$ is an empirical parameter that varies with the heterogeneity of the material. The Freundlich equation is employed to describe heterogeneous systems and reversible adsorption and is not restricted to the formation of monolayer.

The theoretical parameters of adsorption isotherms along with the regression coefficients are listed in Table 4.

The low R^2 values indicated that the Freundlich model was not able to adequately describe the relationship between the amount of Hg^{2+} adsorbed and its equilibrium concentration in the solution. Alternatively, the Langmuir isotherm model was more applicable in describing the process. The maximum adsorption capacity and Langmuir constant were calculated from the slope and intercept of the linear plot of C_e/q_e versus C_e, which gives a straight line with a slope of $1/q_{max}$ that corresponds to complete monolayer coverage and an intercept of $1/q_{max}b$. The results show that the values of q_{max} increased with increasing temperature for each resin, which is in agreement with the results from the adsorption kinetics study (Section 3.3). The q_{max} values of the three resins were found to decrease in the following order: SiO_2-G2.0 > SiO_2-G1.0 > SiO_2-G3.0, which is consistent with the saturated adsorption results (Section 3.1).

For Langmuir isotherm, a method has been adapted to calculate the dimensionless separation factor (R_L),[35] which effectively determines whether the adsorption is favorable by applying the equation

$$R_L = \frac{1}{1 + K_L C_0} \quad (11)$$

where K_L is the Langmuir constant and C_0 is the highest initial concentration. The value of R_L indicates the type of the isotherm to be either unfavorable ($R_L > 1$), linear ($R_L = 1$), favorable ($0 < R_L < 1$), or irreversible ($R_L = 0$). The calculated separation factors

Table 4. Langmuir, Freundlich, and D-R Isotherm Parameters and Correlation Coefficients for the Adsorption of Hg^{2+} in Ethanol Solution onto SiO_2-G1.0, SiO_2-G2.0, and SiO_2-G3.0 Resins at Different Temperatures

		Freundlich			Langmuir				Dubinin−Radushkevich			
					q_{max}	K_L			ln q_{max}	β	E	
adsorbent	T/K	n	K_F	R^2	mg·g^{-1}	L·mg^{-1}	R_L	R^2	mol·g^{-1}	10^8 mol^2·J^{-2}	kJ·mol^{-1}	R^2
SiO_2-G1.0	278	1.767	6.461	0.7546	254.45	0.00716	0.122	0.9342	−6.22	−0.387	11.37	0.9786
	288	1.927	9.102	0.8084	253.81	0.01004	0.090	0.9677	−6.15	−0.351	11.93	0.9802
	298	1.939	9.708	0.8303	259.74	0.01096	0.083	0.9751	−6.21	−0.323	12.45	0.9727
SiO_2-G2.0	278	1.447	3.346	0.7426	269.54	0.00858	0.104	0.9613	−5.96	−0.476	10.25	0.9814
	288	1.601	5.488	0.7846	278.55	0.01049	0.087	0.9629	−5.86	−0.417	10.95	0.9910
	298	1.681	7.127	0.8173	286.53	0.01234	0.075	0.9750	−5.92	−0.395	11.25	0.9843
SiO_2-G3.0	278	1.738	3.876	0.8028	160.26	0.00775	0.114	0.9735	−6.64	−0.391	11.31	0.9948
	288	1.804	5.595	0.8599	210.08	0.00770	0.115	0.9768	−6.27	−0.381	11.46	0.9763
	298	1.755	5.761	0.8109	235.85	0.00720	0.122	0.9490	−6.36	−0.366	11.69	0.9648

dx.doi.org/10.1021/je200235j |J. Chem. Eng. Data 2011, 56, 4407–4415

Table 5. Thermodynamic Parameters of SiO_2-G1.0, SiO_2-G2.0, and SiO_2-G3.0 for Hg^{2+} at Different Temperatures

adsorbent	T/K	ΔG^0 / kJ·mol^{-1}	ΔH^0 / kJ·mol^{-1}	ΔS^0 / J·mol^{-1}
SiO_2-G1.0	278	−1.91	9.49	10.97
	288	−2.31		
	298	−2.70		
SiO_2-G2.0	278	−2.14	16.96	19.04
	288	−2.83		
	298	−3.52		
SiO_2-G3.0	278	−0.52	15.37	15.84
	288	−1.10		
	298	−1.67		

for the adsorbents at different temperatures are summarized in Table 4. The data clearly show that all of the values of R_L are between 0 and 1, indicating that the adsorption process is favorable.

To determine the nature of the adsorption process as physical or chemical, the equilibrium data were also subjected to the D-R isotherm model. The linear form of the D-R isotherm equation[36] is:

$$\ln q_e = \ln q_{max} - \beta\varepsilon^2 \quad (12)$$

where q_e is the amount of metal ions adsorbed on per unit weight of resin, q_{max} is the maximum adsorption capacity, β is the activity coefficient related to the adsorption mean free energy, and ε is the Polanyi potential ($\varepsilon = RT \ln(1 + 1/C_e)$). The D-R model parameter values are given in Table 4, which shows that the D-R model could also describe the adsorption process. This isotherm was more general than Langmuir isotherm since it did not assume a homogeneous surface or constant sorption potential.[37]

The values of Gibbs free energy E were calculated by using the β values as follows[32]

$$E = \frac{1}{\sqrt{-2\beta}} \quad (13)$$

The E value gives information about the adsorption mechanism, either physical or chemical. If it lies between (8 and 16) kJ·mol^{-1}, the adsorption process takes place chemically, while an E value of < 8 kJ·mol^{-1} indicates the adsorption process proceeds physically.[38] The calculated E values are summarized in Table 4. The results show that the E values for the three resins are between (8 to 16) kJ·mol^{-1}, suggesting that in ethanol solution, the adsorption of Hg^{2+} onto the resins was mainly by chemical adsorption.

Thermodynamic behaviors of the adsorption of Hg^{2+} ions onto the resins were investigated using thermodynamic parameters that included the changes in free energy (ΔG^0), enthalpy (ΔH^0), and entropy (ΔS^0). These parameters were determined by using the following equations, and the results are summarized in Table 5.

$$\Delta G^0 = -RT \ln K_C \quad (14)$$

$$\ln K_C = \frac{\Delta S^0}{R} - \frac{\Delta H}{RT} \quad (15)$$

R is the universal gas constant, T is temperature, and K_C (q_e/C_e) is the distribution coefficient.

On the basis of eq 15, the parameters ΔH^0 and ΔS^0 can be obtained from the slope and intercept of the plot of ln K_C versus $1/T$, respectively.

The negative values of ΔG^0 obtained indicate that the adsorption process was spontaneous. The increase in ΔG^0 value with increasing temperature shows that the adsorption was more feasible at higher temperature. The positive values of ΔH^0 indicate that the adsorption processes were endothermic in nature, which is consistent with the results in Section 3.3. The positive values of ΔS^0 showed an increase in the randomness at the solid−solution interface during the adsorption of Hg^{2+}.

4. CONCLUSIONS

Silica gel based adsorbents functionalized with amino-terminated dendrimer-like PAMAM polymers (SiO_2-G1.0, SiO_2-G2.0, and SiO_2-G3.0) were evaluated for the removal of Hg^{2+} ion from ethanol solution. The adsorption of Hg^{2+} was found to be dependent on temperature, concentration, and contact time.

The results from the static adsorption experiments showed that the adsorption capability of the adsorbent decreased with each successive generation of PAMAM. Thus, SiO_2-G1.0 could remove Hg^{2+} ions more effectively than SiO_2-G2.0 and SiO_2-G3.0. When the adsorbent loading was 30 mg, the removal rate of SiO_2-G1.0 was almost 100 %. However, at higher temperatures (298 K and 288 K), SiO_2-G2.0 adsorbed the highest amount of Hg^{2+} among the three resins. Kinetic studies revealed that the adsorption processes for the three adsorbents could be fitted by the pseudosecond-order kinetic model. The kinetic curves showed that the adsorption process could be divided into two steps. In step I, the rate-limiting step was intraparticle diffusion and became external diffusion in step II. The Langmuir isotherm model was more suitable than Freundlich isotherm model to describe the adsorption isotherm. The mean free energy values obtained from the D-R model indicated that the adsorptions were by chemical adsorption. The calculated thermodynamic parameters indicated the feasibility and endothermic and spontaneous nature of Hg^{2+} adsorption onto the three resins.

AUTHOR INFORMATION

Corresponding Author

*Tel.: +86-535-6699201; e-mail: rongjunqu@sohu.com.

Funding Sources

The authors are grateful for the financial support by the National Natural Science Foundation of China (Grant No. 51073075), Natural Science Foundation of Shandong Province (Nos. 2009ZRB01463, 2008BS04011, Y2007B19), the Nature Science Foundation of Ludong University (Nos. 08-CXA001, 032912, 042920), and the Educational Project for Postgraduate of Ludong University (No. YD05001, Ycx0612).

REFERENCES

(1) Ghaedi, M.; Fathi, M. R.; Shokrollahi, A.; Shajarat, F. Highly selective and sensitive preconcentration of mercury ion and determination by cold vapor atomic absorption spectroscopy. *Anal. Lett.* **2006**, *39*, 1171–1185.

(2) Morel, F. M. M.; Kraepiel, A. M. L.; Amyot, M. The chemical cycle and bioaccumulation of mercury. *Annu. Rev. Ecol. Syst.* **1998**, *29*, 543–566.

(3) Boening, D. W. Ecological effects, transport, and fate of mercury: a general review. *Chemosphere* **2000**, *40*, 1335–1351.
(4) World Health Organization. *International Standards of Drinking Water*; WHO: Geneva, 1971.
(5) Veglio, F.; Beolchini, F. Removal of metals by biosorption: a review. *Hydrometallurgy* **1997**, *44*, 301–316.
(6) Inbaraj, B. S.; Wang, J. S.; Lu, J. F.; Siao, F. Y.; Chen, B. H. Adsorption of toxic mercury(II) by an extracellular biopolymer poly(γ-glutamic acid). *Bioresour. Technol.* **2009**, *100*, 200–207.
(7) Ho, Y. S.; Wang, C. C. Sorption equilibrium of mercury onto ground-up tree fern. *J. Hazard. Mater.* **2008**, *156*, 398–404.
(8) Zhou, L. Y.; Wang, P.; Liu, Z. R.; Huang, Q. W. Characteristics of equilibrium, kinetics studies for adsorption of Hg(II), Cu(II), and Ni(II) ions by thiourea-modified magnetic chitosan microspheres. *J. Hazard. Mater.* **2009**, *161*, 995–1002.
(9) Shafaei, A. F.; Ashtiani, Z.; Kaghazchi, T. Equilibrium studies of the sorption of Hg(II) ions onto chitosan. *Chem. Eng. J.* **2007**, *133*, 311–316.
(10) Tuzen, M.; Sari, A.; Mendil, D.; Soylak, M. Biosorptive removal of mercury(II) from aqueous solution using lichen (*Xanthoparmelia conspersa*) biomass: Kinetic and equilibrium studies. *J. Hazard. Mater.* **2009**, *169*, 263–270.
(11) Wilhlem, S. M.; Bloom, N. Mercury in petroleum. *Fuel Process. Technol.* **2000**, *63*, 1–27.
(12) Liang, L.; Horvat, M.; Danilchik, P. A novel analytical method for determination of picogram levels of total mercury in gasoline and other petroleum based products. *Sci. Total Environ.* **1996**, *187*, 57–64.
(13) Brandao, G. P.; de Campos, R. C.; Luna, A. S. Determination of mercury in gasoline by cold vapor atomic absorption spectrometry with direct reduction in microemulsion media. *Spectrochim. Acta B* **2005**, *60*, 625–631.
(14) Leeper, J. E. Mercury—LNG's problem. *Hydrocarbon Process* **1980**, *59*, 237–240.
(15) Moreira, J. C.; Gushikem, Y. Preconcentration of metal ions on silica gel modified with 3(1-imidazolyl)propyl groups. *Anal. Chim. Acta* **1985**, *176*, 263–267.
(16) Gushikem, Y.; Moreira, J. C. Adsorption of MX_2 (M = Mn, Ni, Cu, Zn, and Cd; X = Cl, Br, and I) and $FeCl_3$ by modified silica surface with imidazolylpropyl group. *J. Colloid Interface Sci.* **1985**, *107*, 70–74.
(17) Filho, N. L. D.; Gushikem, Y.; Polito, W. L.; Moreira, J. C.; Ehirim, E. O. Sorption and preconcentration of metal ions in ethanol solution with a silica gel surface chemically modified with benzimidazole. *Talanta* **1995**, *42*, 1625–1630.
(18) Lessi, P.; Filho, N. L. D.; Moreira, J. C.; Campos, J. T. S. Sorption and preconcentration of metal ions on silica gel modified with 2,5dimercapto-1,3,4-thiadiazole. *Anal. Chim. Acta* **1996**, *327*, 183–190.
(19) Filho, N. L. D.; Marangoni, F.; Mendonça Costa, R. Preparation, characterization, and CuX_2 and CoX_2 ($X = Cl^-$, Br^-, ClO^{-4}) adsorption behavior of a polyhedral oligomer silsesquioxane functionalized with an organic base. *J. Colloid Interface Sci.* **2007**, *313*, 34–40.
(20) Zeng, F.; Zimmerman, S. C. Dendrimers in Supramolecular Chemistry: From Molecular Recognition to Self-Assembly. *Chem. Rev.* **1997**, *97*, 1681–1712.
(21) Bosman, A. W.; Janssen, H. M.; Meijer, E. W. About Dendrimers: Structure, Physical Properties, and Applications. *Chem. Rev.* **1999**, *99*, 1665–1688.
(22) Esumi, K.; Hosoya, T.; Suzuki, A. Formation of Gold and Silver Nanoparticles in Aqueous Solution of Sugar-Persubstituted Poly(amidoamine) Dendrimers. *J. Colloid Interface Sci.* **2000**, *226*, 346–352.
(23) Qu, R.; Niu, Y.; Sun, C.; Ji, C.; Wang, C.; Cheng, G. Syntheses, characterization, and adsorption properties for metal ions of silica-gel functionalized by ester- and amino-terminated dendrimer-like polyamidoamine polymer. *Microporous Mesoporous Mater.* **2006**, *97*, 58–65.
(24) Rengaraj, S.; Arabindoo, B.; Murugesan, V. Sorption characteristics of Parachlorophenol on activated palm seed carbon. *Indian J. Environ. Health* **1999**, *41*, 16–23.
(25) Rengaraj, S.; Sivabalan, R.; Arabindoo, B.; Murugesan, V. Adsorption kinetics of o-cresol on activated carbon from palm seed coat. *Indian J. Chem. Technol.* **2000**, *7*, 127–131.
(26) Wang, S.; Li, H. Dye adsorption on unburned carbon: kinetics and equilibrium. *J. Hazard. Mater.* **2005**, *26*, 71–77.
(27) Tütem, E.; Apak, R.; Ünal, C. F. Purification of water by activated carbons from apricot stones, lignites and anthracite. *Water Res.* **1998**, *32*, 2315–2139.
(28) Ho, Y. S.; McKay, G. Pseudo-second order model for sorption processes. *Process Biochem.* **1999**, *34*, 451–465.
(29) Aroua, M. K.; Leong, S. P. P.; Teo, L. Y.; Yin, C. Y.; Daud, W. M. A. W. Real-time determination of kinetics of adsorption of lead(II) onto palm shell-based activated carbon using ion selective electrode. *Bioresour. Technol.* **2008**, *99*, 5786–5792.
(30) Weber, W. J.; Morris, J. C. Kinetics of adsorption on carbon from solution. *J. Sanit. Eng., Div. Am. Soc. Civ. Eng.* **1963**, *89*, 31–60.
(31) Wu, Z.; Joo, H.; Lee, K. Kinetics and thermodynamics of the organic dye adsorption on the mesoporous hybrid xerogel. *Chem. Eng. J.* **2005**, *112*, 227–236.
(32) Helfferich, F. *Ion-Exchange*; McGraw-Hill: New York, 1962.
(33) Mohan, D.; Gupta, V. K.; Srivastava, S. K.; Chander, S. Kinetics of mercury adsorption from wastewater using activated carbon derived from fertilizer waste. *Colloids Surf., A* **2001**, *177*, 169–181.
(34) Weber, W. J.; DiGiano, F. A. *Process dynamics in environmental systems*; John Wiley & Sons, Inc.: New York, 1996.
(35) Ozacar, M.; Sengil, I. A. Adsorption of reactive dyes on calcined alunite from aqueous solutions. *J. Hazard. Mater.* **2003**, *B98*, 211–224.
(36) Dubinin, M. M.; Zaverina, E. D.; Radushkevich, L. V. Sorption and structure of active carbons. I. Adsorption of organic vapors. *Zh. Fiz. Khim.* **1947**, *21*, 1351–1362.
(37) Ozlem, C.; Demet, B. Adsorption of some textile dyes by hexadecyltrimethylammonium bentonite. *Turk. J. Chem.* **2001**, *25*, 193–200.
(38) Kiran, I.; Akar, T.; Ozcan, A. S.; Ozcan, A.; Tunali, S. Biosorption kinetics and isotherm studies of Acid Red 57 by dried *Cephalosporium aphidicola* cells from aqueous solutions. *Biochem. Eng. J.* **2006**, *31*, 197–203.